

# Atomic Resolution Transmission Electron Microscopy of the Intergranular Structure of a $Y_2O_3$ -Containing Silicon Nitride Ceramic

A. Ziegler,<sup>†</sup> C. Kisielowski,<sup>‡</sup> M. J. Hoffmann,<sup>\*,§</sup> and R. O. Ritchie<sup>†</sup>

Materials Sciences Division, Lawrence Berkeley National Laboratory, and  
Department of Materials Science and Engineering,  
University of California, Berkeley, California 94720

National Center for Electron Microscopy, Lawrence Berkeley National Laboratory, Berkeley, California 94720

Institut für Keramik im Maschinenbau, Universität Karlsruhe, D-76131 Karlsruhe, Germany

**High-resolution transmission electron microscopy (HRTEM) employing focus-variation phase-reconstruction methods is used to image the atomic structure of grain boundaries in a silicon nitride ceramic at subangstrom resolution. Complementary energy-dispersive X-ray emission spectroscopy experiments revealed the presence of yttrium ions segregated to the 0.5–0.7-nm thin amorphous boundary layers that separate individual grains. Our objective here is probing if yttrium ions attach to the prismatic planes of the  $Si_3N_4$  at the interface toward the amorphous layer, using Scherzer and phase-reconstruction imaging, as well as image simulation. Crystal structure images of grain boundaries in thin sample ( $<100$  Å) areas do not reveal the attachment of yttrium at these positions, although lattice images from thicker areas do suggest the presence of yttrium at these sites. It is concluded that most of the yttrium atoms are located in the amorphous phase and only a few atoms may attach to the terminating prism plane. In this case, the line concentrations of such yttrium in the latter location are estimated to be at most one yttrium atom every 17 Å.**

## I. Introduction

BULK silicon nitride ( $Si_3N_4$ ) ceramics have been the subject of numerous investigations, in particular because their physical and mechanical properties are relevant for many potential high-temperature applications. However, the properties of silicon nitride ceramics are strongly influenced by the microstructure and the chemical composition of the grain boundaries. Indeed, the grain boundaries can be considered as the key microstructural features that control mechanical properties. For example, at low homologous temperatures, a strongly bonded grain boundary can result in high strength, but a suitably “weakened” boundary, e.g., from the presence of a brittle intergranular film, invariably results in higher toughness. Similarly, at high temperatures, a grain-boundary phase with a higher melting point or high viscosity is preferable for strength retention and creep resistance.

In most silicon nitride ceramics, the ubiquitous thin grain boundaries are typically 1–5 nm in width, with their equilibrium size considered to be a marked function of chemical composition.<sup>1–6</sup> Sintering additives and impurities, particularly rare earths,<sup>¶</sup> segregate along such boundaries<sup>7</sup> and generally do not form solid solutions with either the  $\alpha$ - or  $\beta$ -phase  $Si_3N_4$  matrix. However, they are thought to somehow bond to the matrix grain’s prism plane along the interface with the grain boundary phase.

A variety of  $Si_3N_4$  interface models have been published.<sup>8–14</sup> Using a Hartree–Fock periodic approach with extended Hückel tight-binding approximation<sup>8,9</sup> and molecular dynamic calculations with a pair-potential set approach,<sup>10</sup> atomic positions and grain-boundary bonding characteristics have been determined for a variety of interface–atom coordinations. Of particular interest for this investigation is the chemical bonding between the prismatic plane of a silicon nitride grain and atoms of sintering additives that has been modeled computationally using crystal structure data. Dudesek and Benco<sup>8,9</sup> work with an oxygen-terminated prism plane, whereas Nakayasu *et al.*<sup>10</sup> and Painter *et al.*<sup>11</sup> work with one that is nitrogen-terminated. Both models allow for sintering-aid atoms to attach to this type of interface plane. These O- and N-terminated interfaces provide the basis for the image simulations conducted in this investigation. The two theoretical approaches are realistic if one considers that most, if not all, of these thin grain boundaries are found to contain oxygen. Thus, all or some Si–N bonds could have been replaced by Si–O bonds, and oxygen could have taken the atom positions of nitrogen resulting in a fully or partially O-terminated prism plane. The idea of substituting oxygen for nitrogen can also be interpreted as an oxynitride monolayer, and it also satisfies the conception that yttrium is a priori linked to oxygen as sintering additive  $Y_2O_3$ .

Both models also support segregation of sintering aids to the grain boundaries. Benco<sup>9</sup> states that oxygen present along grain boundaries in  $Si_3N_4$  has a destabilizing effect on the bonding characteristics if associated antibonding interactions are not prevented. Therefore, oxygen can be seen as serving as a trap for sintering aids to migrate toward the grain boundaries. The results of Nakayasu *et al.*<sup>10</sup> demonstrate how  $Ln^{3+}$  ions are more stable at the interfaces and less stable in the  $Si_3N_4$  matrix. These results are consistent with experimental observations.

However, direct imaging, e.g., using high-resolution transmission electron microscopy (HRTEM), of the crystal structure at the interfacial regions, specifically to identify the positions of the additive ions, has not been achieved with truly atomic resolution. A major problem here has been that a point-to-point resolution of  $\leq 0.93$  Å is required to identify single-atom columns in  $Si_3N_4$ , and this is close to the theoretical information limit of current electron microscopes. Secondly, the imaging of grain boundaries in silicon

D. R. Clarke—contributing editor

Manuscript No. 186955. Received May 22, 2002; approved May 27, 2003.

This work was supported by the Director, Office of Science, Office of Basic Energy Sciences, Division of Materials Sciences and Engineering of the U.S. Department of Energy under Contract No. DE-AC03-76SF00098.

<sup>¶</sup>Member, American Ceramic Society.

<sup>†</sup>Materials Sciences Division, Lawrence Berkeley National Laboratory, and University of California, Berkeley.

<sup>‡</sup>National Center for Electron Microscopy, Lawrence Berkeley National Laboratory.

<sup>§</sup>Universität Karlsruhe.

<sup>¶</sup>Exceptions here are the  $\alpha$ - and  $\beta$ -SiAlON structures, which are isostructural derivatives of  $\alpha$ - and  $\beta$ - $Si_3N_4$ .

nitride is further complicated by the formation of a thin amorphous film at the interface. Crystallization of the majority of this interfacial phase at boundary triple junctions is commonly reported, although, for the more interesting thin two-grain grain-boundary films, the amorphous state has been shown to be the thermodynamically preferred condition.<sup>15</sup>

Recent progress with HRTEM, however, has made it possible to extend the resolution of a “mid-voltage” microscope well beyond its Scherzer point-to-point resolution of 1.7 Å to an information limit of about 0.8 Å.<sup>16–19</sup> The procedure is based on several studies<sup>18–31</sup> and exploits the small information limit of a field emission TEM in a particular manner via digital image processing<sup>32,33</sup> to produce electron exit waves. Usually, a single HRTEM image represents a highly encoded mixture of the properties of the sample with those of the TEM. A reconstruction of the electron exit wave from a focus series of lattice images, on the other hand, allows eliminating imaging artifacts, extending resolution, and simplifying image interpretation.

In this paper, we use this technique to image silicon nitride with an unprecedented resolution and a sensitivity that allows for the detection of single nitrogen columns in the Si<sub>3</sub>N<sub>4</sub> matrix. Specifically, we focus on the grain boundaries in a silicon nitride sintered with 2 wt% Y<sub>2</sub>O<sub>3</sub> and examine the segregation of the sintering additive ions to these interfaces. It is found that although the yttrium ions definitely segregate to the boundaries, it was difficult to detect irrefutable evidence that the yttrium ions attach to the prism plane of the half-ring of the Si hexagons that are present, we believe, because the yttrium ion concentration in these locations was too low.

## II. Experimental Procedure

### (1) Material

The silicon nitride examined was fabricated with a newly developed two-step sintering technique, consisting of a dilatometer-controlled, gas-pressure-sintering process and a subsequent hot-isostatic pressing densification.<sup>34</sup> Such highly pure and controlled processing was used to permit an unambiguous investigation of the role of small quantities of sintering aids that optimize the material properties; specifically, the technique allowed for an almost impurity-free densification without the usual glass encapsulation technique.

Si<sub>3</sub>N<sub>4</sub> powder (UBE SN E10; Ube Industries, Yamaguchi, Japan) was sintered with 2 wt% Y<sub>2</sub>O<sub>3</sub> (fine grade, HCST) to achieve a microstructure consisting of two morphologies of β-Si<sub>3</sub>N<sub>4</sub> grains, namely, (i) predominantly acicular-shaped grains, with an average length of 5 μm and an aspect ratio of 8:1, and (ii) equiaxed grains, with a size of 0.5–1.5 μm. No particular postsintering heat treatment was performed on this material. An image of the microstructure is shown in Fig. 1.

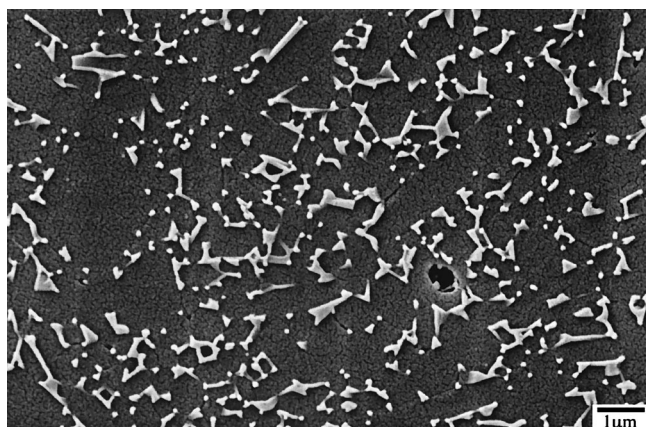


**Fig. 1.** Morphology of the microstructure of the 2-wt%-Y<sub>2</sub>O<sub>3</sub>-containing Si<sub>3</sub>N<sub>4</sub> ceramic, showing the predominantly acicular-shaped β-Si<sub>3</sub>N<sub>4</sub> grains.

Samples for examination in the TEM were prepared by grinding, dimpling, and ion milling. The low-voltage ion milling was performed with an ion mill (Technoorg LINDA, IV3H/L ion beam thinning unit, Scientific Technical Development Ltd., Budapest, Hungary) to produce foils with a thickness of <100 Å and with highly smooth surfaces (i.e., surface roughness ≤10 Å).

### (2) Electron Microscopy

(A) *Electron Microscope:* The HRTEM investigation was performed with a Philips CM300/FEG/UT, a 300-kV microscope, equipped with a field emission electron source (FEG), and an ultra-twin-objective lens of low spherical aberrations ( $C_s = 0.60$  mm) and chromatic aberrations ( $C_c = 1.3$  mm). Partial aberration correction reduces image distortion to about its information limit of 0.8 Å.<sup>35</sup>

The specimen stage used was a Philips double-tilt low-background holder with a tilting range of  $\pm 30^\circ/\pm 30^\circ$ . Images were recorded digitally through an attached Gatan Image Filter (GIF) on a 2048- × 2048-pixel CCD (charge-coupled device) camera that allows for a total magnification up to 38 million times. Electron exit waves were reconstructed from a series of 20 lattice images using the Philips/Brite-Euram software by Coene and Thust.<sup>32,33</sup>

(B) *Phase Retrieval and Image Reconstruction:* Subangstrom resolution was achieved by exploiting the high information limit of the TEM via digital image processing.<sup>16–19</sup> Phase retrieval and focal series reconstruction allows elimination of imaging artifacts and undesired effects of delocalization that complicate the interpretation of single images. The phase of the electron exit waves was typically extracted from 20 lattice images recorded around an underfocus of -260 nm with a constant defocus interval of ~2.4 nm for successive lattice images.

(C) *Analytical Equipment:* Analytical investigations of the distribution of chemical elements along the grain boundary were performed on a Philips CM200/FEG transmission electron microscope. This analytical TEM is equipped with an energy dispersive X-ray emission spectrometer (EDS). Spatially resolved compositional analysis ( $Z > 5$ ) could be performed with this instrument with an energy resolution of 136 eV for MnK $\alpha$  radiation. The EDS probe diameter could be focused to a 1.2 nm small spot to detect the signal emanating from a 1 to 5 nm thick two-grain grain-boundary film.

### (3) Computer Simulations

The crystal structure and interface modeling was performed using the commercial program CrystalKit.<sup>36</sup> Subsequent HRTEM image simulations were performed using the structure models as input to the commercial program MacTempas.<sup>36</sup> Through-focus and through-thickness image simulations can be created with this program from the model crystal structures. MacTempas is based on the multislice method where the structure model is sliced perpendicular to the direction of the incident beam. The crystal potential content of each single slice modifies the incoming electron wave as do all successive slices through the entire structure model.<sup>37</sup>

## III. Results and Discussion

Demonstration of the resolution and capabilities of the microscope and the approach to exit-wave phase reconstruction can be found in various publications<sup>17–19,21–23,27–33</sup>

### (1) Experimental Images

To study the atomic structure of the grain boundaries in Si<sub>3</sub>N<sub>4</sub>, thin grain boundaries were examined using the exit-wave reconstruction process. This technique proved to be successful in particular for imaging the intergranular phase on a very thin specimen, i.e., ≤100 Å thick. Foils much thicker than 100 Å did not turn out to be optimal for phase reconstruction, due to loss of resolution (for reasons that are under investigation). Nevertheless,

images of specimen areas thinner and thicker than this desired limit are presented, since they both carry complementary information about grain boundaries. The results are described below in terms of current theoretical models<sup>8-11</sup> for the interfacial structure of silicon nitride. We would like to emphasize that the results focus only on the immediate atom attachment at the  $Si_3N_4$ -prism plane facing the grain boundary.

(A) *Scherzer and Reconstructed Phase Images in Thin Specimen ( $\leq 100$  Å):* The results of phase reconstructed exit-wave images of thin boundaries are presented in Figs. 2(a) and 3(a) and are compared with corresponding Scherzer defocus images in Figs. 2(b) and 3(b). A significant gain in information is apparent since the phase reconstructed images depict the crystal structure directly. In both examples, a residual tilt of 0.87 and 1.05 mrad can be detected which affects the intensity distribution in the lattice images and the reconstructed electron exit wave. Experimental parameters, specifically, defocus,  $\Delta f$ , and sample thickness,  $t$ , in these sampling areas were determined via comparison of the Scherzer images to computer-simulated images. In Fig. 2,  $\Delta f = -50$  nm and  $t \sim 10-20$  Å, whereas, for Fig. 3,  $\Delta f = -70$  nm and  $t \sim 70-80$  Å. In interpreting these images, it can be deduced that the grain boundary is amorphous and  $\sim 5-7$  Å in thickness. Preferential etching during specimen preparation could not be observed (Fig. 4.). The precise determination of the grain boundary thickness is not further addressed in this investigation. We acknowledge, however, that it is important for the understanding of the atomic structure bridging the entire grain boundary.

Figure 2(a) shows the remarkable shape of the  $Si_3N_4$  hexagons in the  $\beta$ - $Si_3N_4$  grain to the right that reach into the amorphous

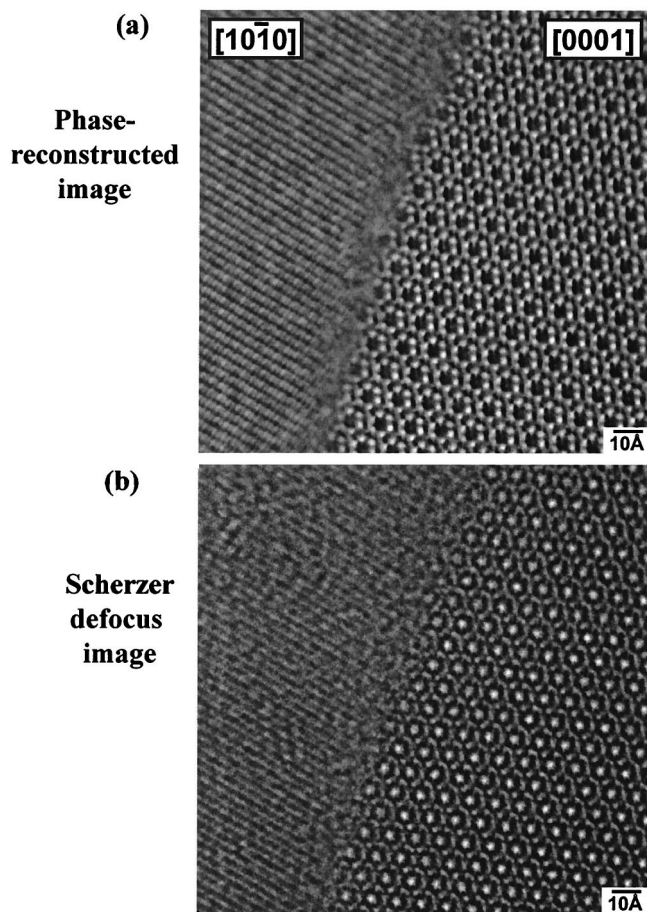


**Fig. 2.** Phase-reconstructed (a) and the corresponding Scherzer defocus images (b) of a grain boundary. The thickness in this sample area can be determined to 10–20 Å. Note the shape of the  $Si_3N_4$  hexagons in the phase-reconstructed image; they are not fully closed and extend into the amorphous phase. The thickness of the amorphous grain-boundary layer can be approximated as 5–7 Å.

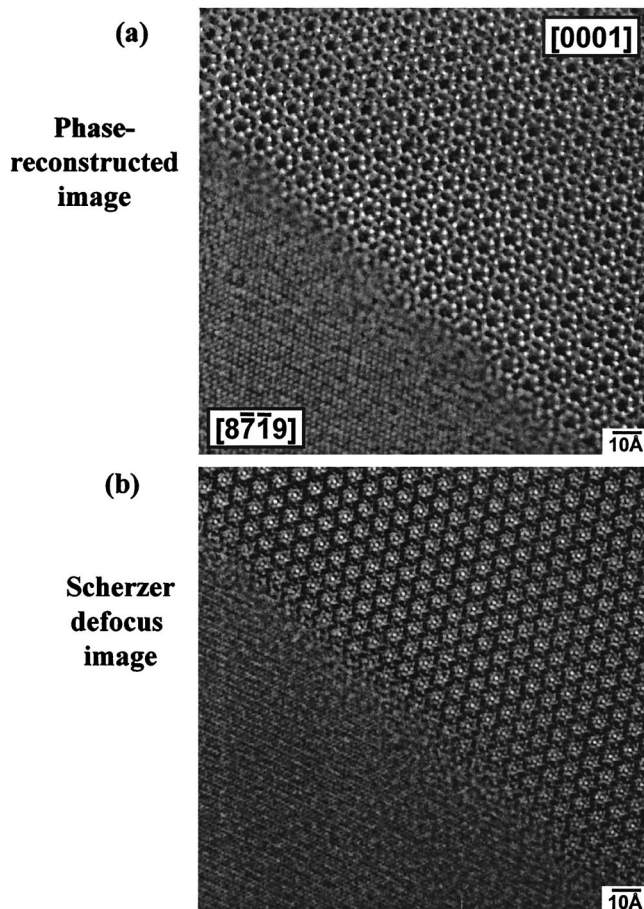


**Fig. 3.** Phase-reconstructed (a) and corresponding Scherzer defocus images (b) of a second grain boundary in a thicker sample area. Sample thickness is determined to 70–80 Å.

intergranular layer. The reconstructed image reveals rather incomplete, not fully closed, hexagon rings extending into the amorphous grain boundary. This observation suggests the possibility of dangling bonds connecting the  $\beta$ - $Si_3N_4$  grain to segregated ions in the amorphous grain boundary. However, no segregated sintering additive ions can be identified in these reconstructed images at any particular atom-column position along the interface.

(B) *Scherzer and Reconstructed Phase Images in Thick Specimen ( $\geq 100$  Å):* The Scherzer and phase-reconstructed exit-wave images of a grain boundary in a slightly thicker sample area are presented in Figs. 5(a) and (b), respectively. The image parameters here are  $\Delta f = -60$  nm and  $t \sim 120-130$  Å. In contrast to the Scherzer images of the thin sample, the corresponding image in the thicker sample area displays bright spots that are arranged in a periodic manner close to the prismatic plane. Additionally, the resulting phase reconstructed image reveals that the bright spots disappear and the half-rings of the Si hexagons vanish, unlike the images taken of thinner sample areas. This outcome is attributed to the presence of interface roughness, and it is tempting to assign the occurrence of the regular intensity spots in the Scherzer image of Fig. 5(a) to delocalization. However, image simulations did not reproduce these additional regular intensity spots in Scherzer images unless heavy elements are introduced as part of the interface (Fig. 6). In this case, substituting, for example, silicon atoms for the heavier element yttrium does not result in bright spots in the image simulations. Moreover, private communications<sup>38</sup> with other TEM microscopists investigating  $Si_3N_4$  coincide with our observation, and bright periodic spots along the grain boundaries in silicon nitride have been observed in the past. To date, it seems that their appearance is not necessarily due to any specific type of electron emission source used in a TEM.

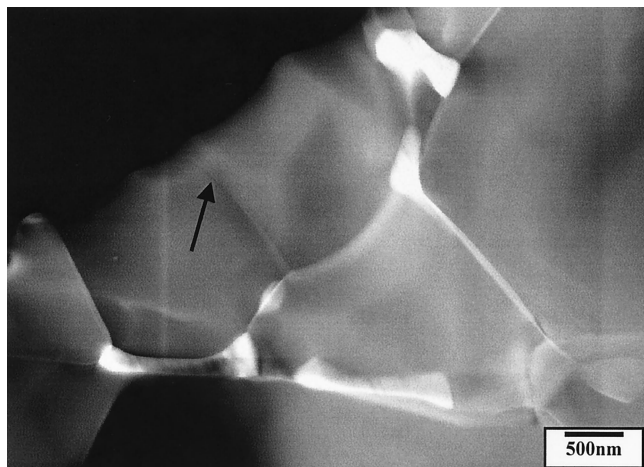


**Fig. 4.** TEM image of a grain boundary ending into the specimen perforation (arrow). The sample is very thin at this location ( $< 50 \text{ \AA}$ ). Nevertheless, there is no sign of preferential etching of the grain boundary during specimen preparation.

The question is how to combine and interpret the visual information revealed in these images of thin and thick specimen areas and what conclusions can be drawn from this about the near-prism plane interface structure in  $\text{Si}_3\text{N}_4$ . We know that the heavy element is yttrium. It can possibly be attached to the prismatic plane. However, salient criteria and imaging conditions must be met to identify atom segregation along the interface and allow image interpretation. Of greatest interest is the yttrium-ion concentration, that is, the ion-column density. Other criteria are specimen thickness and electron oscillation wavelength, both of which are addressed below in Section III(2)(A).

Because the  $\text{Si}_3\text{N}_4$  investigated here contains only a small amount (2 wt%) of  $\text{Y}_2\text{O}_3$ , it was necessary to confirm that sufficient yttrium ions were present along boundaries; this was achieved using an EDS line scan taken across the thin grain boundaries. The results, shown in Fig. 7, clearly demonstrate that yttrium is segregated to the interface. However, not all the ions detected via EDS are believed to be attached in columns to the prism planes. In fact, it is expected that most of the yttrium atoms are located in the amorphous phase and only a few atoms are attached to the prism plane of the matrix grain–grain boundary interface.

Since yttrium is a heavier atom than silicon and nitrogen, this should yield stronger electron scattering and image contrast, e.g., brighter spots, and would enable detection of individual yttrium atoms along the grain boundary. Moreover, for imaging it is the density of these ions attached to the prism plane in a column parallel to the direction of the incident electron beam that is important. A denser column of ions causes stronger scattering of the incident electrons. However, neither the Scherzer nor the phase-reconstructed images in Figs. 2 and 3 exhibit such brighter spots at any location along the prismatic planes. For phase-reconstructed exit-wave imaging, a low column density can be a problem. Especially, if the bonding characteristics are such that there is a large separation between yttrium ions attached to the prism plane along the columns, this requires using a thicker sample to exceed a minimum ion density for good imaging contrast. This, however, can conflict with the upper desired limit of  $100 \text{ \AA}$  for optimal resolution when using the phase-reconstruction method. We assume a low ion concentration to be the reason why images taken on thin specimen areas (Figs. 2 and 3) do not show any signs of yttrium. However, just because yttrium atoms cannot be seen in the phase-reconstructed exit-wave images does not automatically imply a complete absence of yttrium atoms at the prism plane interface, especially when Fig. 6 shows that yttrium can cause the bright spots, as are observed in the experimental Scherzer image in Fig. 5(a).

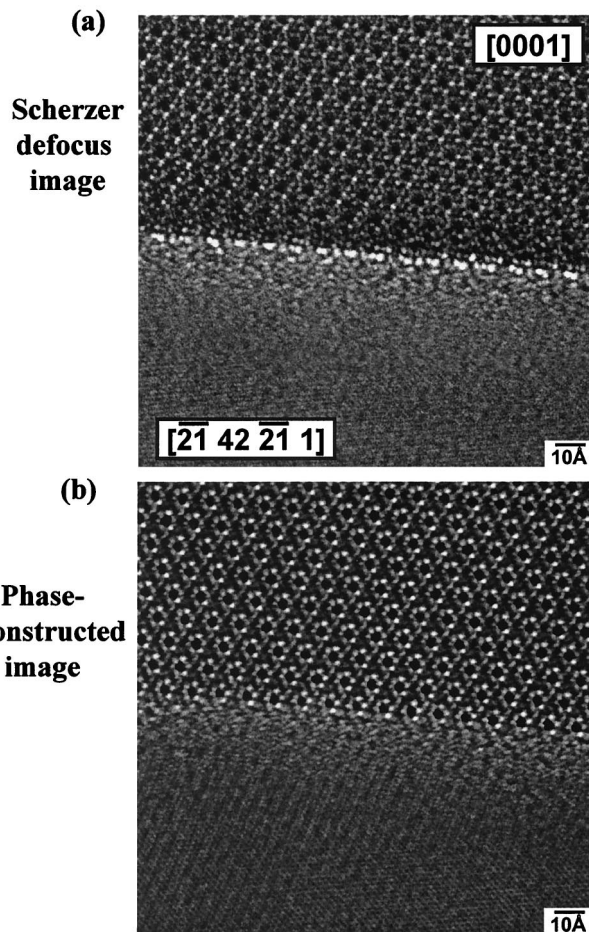


**Fig. 5.** Scherzer defocus (a) and corresponding phase-reconstructed images (b) of a grain boundary. The sample in this area is estimated to be thicker ( $120\text{--}130 \text{ \AA}$ ) than the recommended specimen thickness for optimum phase-reconstruction results. The Scherzer image displays bright spots that exhibit a very regular periodicity. These features disappear though in the phase-reconstructed image.

Such experimental results are discussed below in light of the image simulations that are based on the theoretical assumptions regarding the near-matrix grain structure.<sup>8–11</sup> Of primary interest is the ion-column density.

## (2) Simulated Images

(A) *Exit-Wave Image Simulation of Grain Boundaries:* The basis for the present image simulations are the models set forth by Dudesek and Benco,<sup>8,9</sup> Nakayasu *et al.*,<sup>10</sup> and Painter *et al.*:<sup>11</sup> an O- or N-terminated prismatic plane serving as the interface between the matrix grain and the grain boundary. The two models differ only in the type of atom that terminates the prism plane. It is therefore very difficult to differentiate in HRTEM images, e.g., Figs. 2 and 3, whether the  $\text{Si}_3\text{N}_4$ -hexagon half-rings reaching into the amorphous grain boundary are O- or N-terminated since both elements are close in atomic weight and scattering power. Hence, the contrast in image simulations is not affected by what type of atom terminates the prism plane.

However, when performing image simulation, some additional imaging criteria have to be taken into consideration. These include specimen thickness and electron oscillation wavelength in the specimen.<sup>39</sup> Both, and in particular their combined effects, determine conditions for imaging atoms. In this case for the sintering-aid ions along the grain boundary, it can affect whether atoms will be visible (or disappear) in a simulated exit-wave image.

Attempts were made to simulate TEM images of this near-interface structure and compare them to the experimental images. One has to keep in mind, though, that, with simulated images, there is always much better detail visible than with corresponding

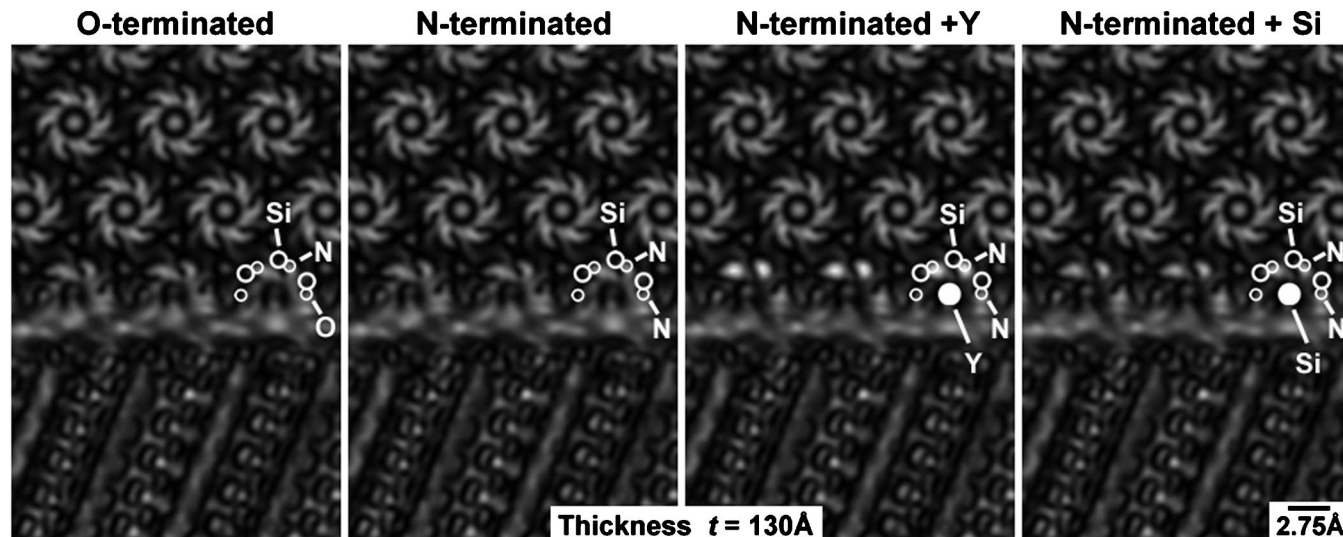


**Fig. 6.** Simulated Scherzer defocus images showing that there is no difference between the images when using an oxygen- or a nitrogen-terminated prism plane. When attaching on either the O- or N-terminated prism plane the atoms yttrium or silicon, there is a difference in the resulting Scherzer image. Yttrium causes bright periodic spots to appear, while silicon does not produce such bright spots.

experimental images. The objective is (i) to identify any possible attachment of sintering-aid ions to the prism planes and (ii) to determine what the ion-column density and specimen thickness requirements are. To this end a variety of image simulations were conducted using the following model structure: two opposing  $Si_3N_4$  matrix grains, one oriented along [0001] and the other with no particular preferred orientation, were connected with an amorphous grain boundary, a few angstroms thick and containing yttrium atoms attached to the prism plane of the [0001]-oriented grain. The yttrium ion-column density was varied by changing the relative separation between Y atoms, from one yttrium atom every 2.8 Å to one yttrium atom every 19.6 Å (2.8 Å is the  $Si_3N_4$  unit cell dimension in [0001]). The sample thickness was then varied for each ion-column density from 10 to 130 Å. This allowed for an examination of the present Bloch wave oscillations on the exit-wave image.

A selection of the simulated images is presented in Fig. 8. The images shown correspond to three different ion-column densities: one yttrium ion every 2.8, 5.6, and 16.8 Å, respectively. The intensity differences between the Si, N, and Y atoms are noticeable

and due to the atomic weight and scattering power of each element (Fig. 9). One can also see that the highly dense Y-ion column displays the brightest spots. However, for the less dense ion columns, the yttrium signal weakens. In fact, at an ion-column density of 16.8 Å, the yttrium signal is weaker than the nitrogen intensity (Fig. 9). Furthermore, it is noteworthy that the intensity of the yttrium signal clearly varies with specimen thickness. This behavior can be explained by the interaction of the varied parameters, i.e., the Bloch wave oscillation.

The Bloch wave oscillation is caused by the interaction of the incoming electron waves with material in zone axis orientation and is strongly dynamic. The propagating electron wave exhibits a specific distance—an extinction distance  $\zeta$ —that depends on the scattering power of a specific column of atoms. Lighter atoms produce a longer extinction distance compared with heavier atoms. Moreover, the extinction distance scales with  $d^2/Z$ , where  $d$  is the atom separation and  $Z$  is the atomic number.<sup>39</sup> The combination of this effect with specimen thickness governs the visibility of atoms. Maximum image contrast and thus visibility at the exit plane occur when the specimen thickness coincides with half of an extinction

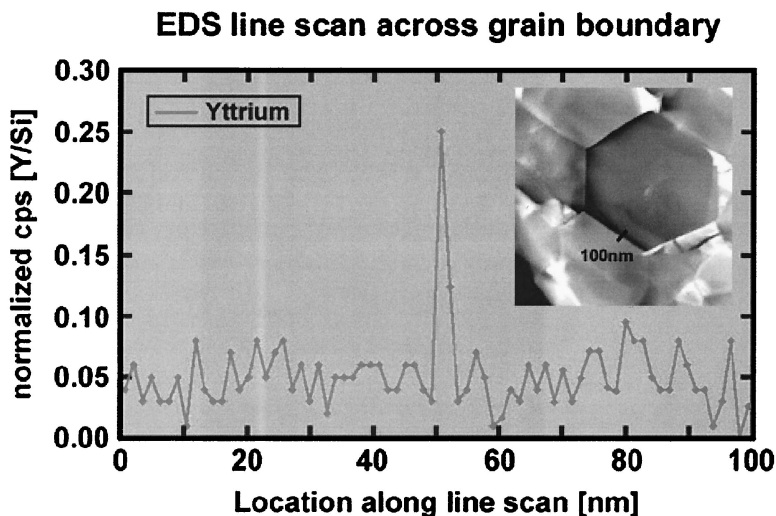


**Fig. 7.** EDS line scan taken across a thin grain boundary reveals the presence of yttrium ions segregated to the amorphous interface layer. The grain-boundary thickness is difficult to determine with this signal, since the EDS probe size is 1.2 nm and only one location definitely detects yttrium. It is expected that most of these Y ions are not attached to the prism plane; instead they are located in the thin amorphous grain-boundary layer.

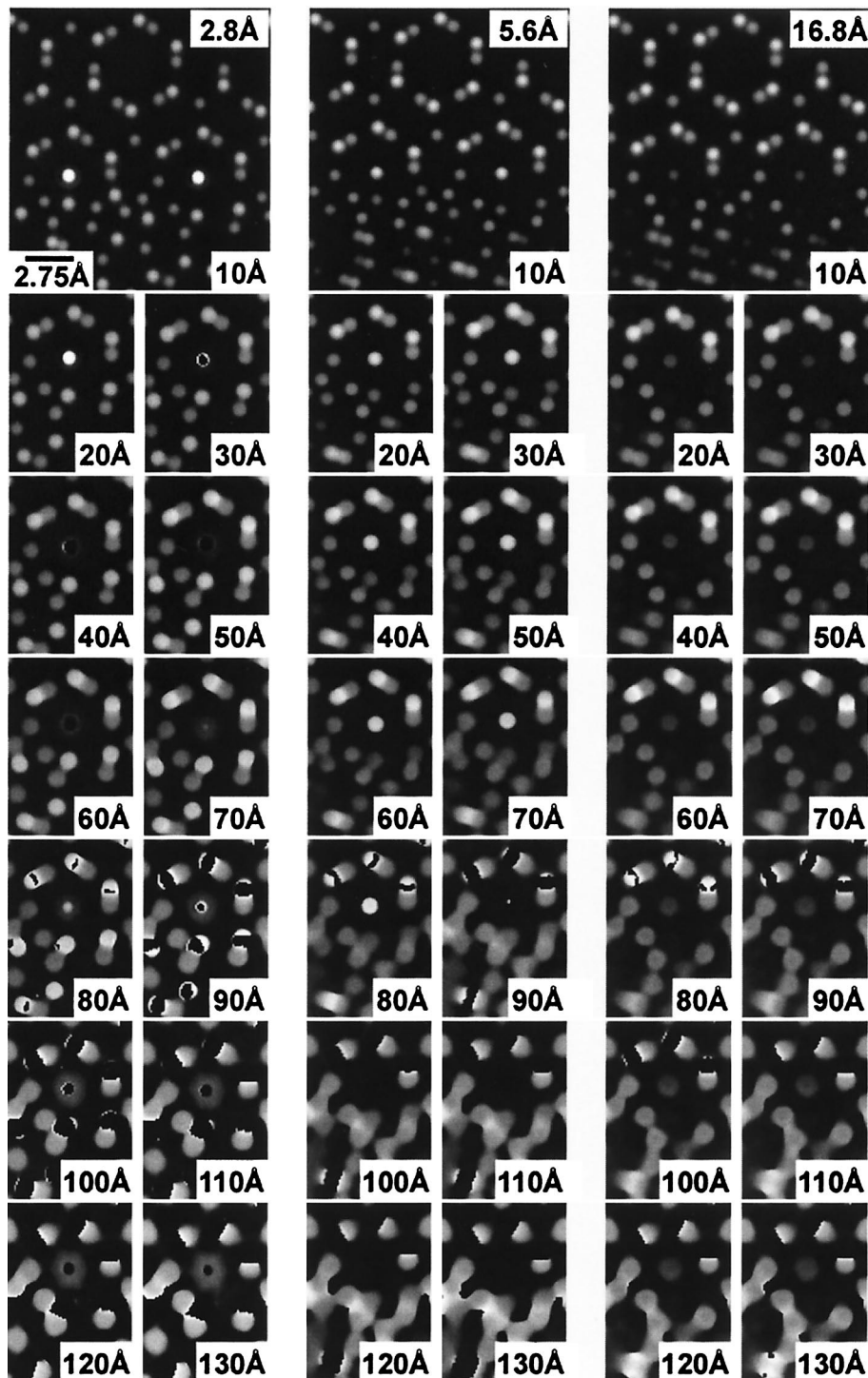


**Fig. 8.** Array of simulated exit-wave images depicting the nitrogen-terminated  $\text{Si}_3\text{N}_4$  half-rings containing yttrium ions that reach into the amorphous grain-boundary region. Evidence of electron-wave oscillation in relationship to specimen thickness can be seen in the intensity variations, in particular, of the Si and the Y signals.

oscillation. The approximated half-extinction distance for a column of Si atoms with a density of one Si atom/(2.8 Å) is  $\zeta \sim 75$  Å.<sup>40</sup> In comparison, the extinction distance for yttrium is approximated to  $\zeta \sim 26$  Å and  $\zeta \sim 104$  Å at a separation of 2.8 Å and 5.6 Å, respectively.

A phenomena introduced by image simulation programs is phase wrapping, which means that instead of having a continuous sinusoidal-like variation in intensity, there is a jump every  $2\pi$ . This causes the intensity to abruptly change from a bright white spot to a black spot. One can see this phase wrapping in the image simulations in Fig. 8, and it can be used to easily determine the point at which a spot's intensity reaches its maximum and starts to

decline again, in evidence of the electron oscillation wavelength and in accordance with previous work.<sup>39,40</sup>

On the basis of this, the intensity variations observed in Fig. 8 can be better interpreted. If, for example, the yttrium ion-column separation were to be 2.8 Å/Y ion and the extinction distance  $\sim 26$  Å, then the yttrium signal would be strongest at a specimen thickness of  $\sim 20$ – $30$  and  $\sim 70$ – $80$  Å but vanish at a specimen thickness of  $\sim 50$ – $60$  Å. Comparing this to the experimental images at thicknesses of 10–20 and 70–80 Å in Figs. 2 and 3, respectively (which show no yttrium), permits the conclusion that the prism planes are not as densely populated with yttrium. A similar conclusion applies to an ion-column density of one yttrium

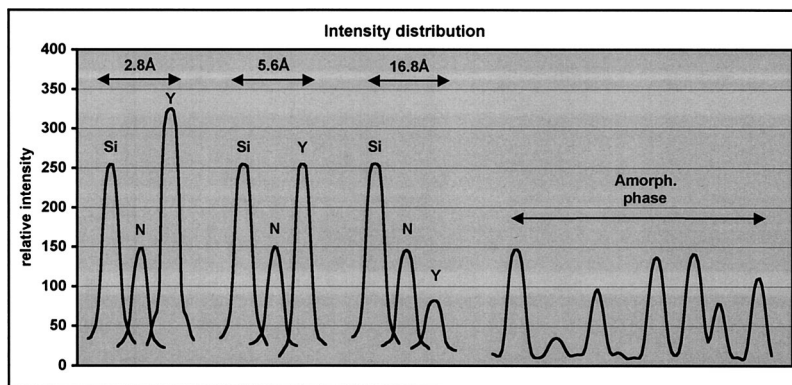


**Fig. 9.** Intensity distribution for Si, N, and Y in simulated images at three different ion-column densities (distance between Y ions: 2.8, 5.6, and 16.8 Å) and of the amorphous grain-boundary phase. The intensity of the yttrium signal changes significantly with ion-column density and falls below the average intensity level of the amorphous phase, with the consequence of the yttrium atoms becoming invisible.

every 5.6 Å. The Y signal intensity would be at maximum at 90–100 Å and therefore most likely also visible at 70–80 Å, unlike Fig. 3. Continuing this process, one can determine a lower visibility limit, i.e., at what ion-column density the yttrium signal will vanish. For this case, this limit appears to be at an yttrium ion-column density of 16.8 Å. Moreover, one has to consider also the fact that not only the extinction distance eliminates a signal, but any atom signal will become invisible when it is comparable to the noise level, represented here by the amorphous intergranular phase (Fig. 9).

These results help explain why yttrium cannot be detected in the thin (<100 Å) experimental phase-reconstructed images shown in Figs. 2 and 3, because the line density is too low. Yttrium can be attached to the prism planes, according to theoretical predictions, but these prism planes are most likely only very sparsely populated with yttrium ions; otherwise they would be visible. Accordingly, we turn to the experimental images taken from thicker sample areas (>100 Å) to attempt to identify the potential yttrium attachment to the prism planes.

The exit-wave image simulations in Fig. 8 show how difficult it can become to interpret and decipher the images when specimen thickness is increased. Similar difficulties arise in the experimental phase-reconstructed exit-wave images that are primarily due to loss of resolution. No yttrium atoms and no  $Si_3N_4$  half-rings can be detected anymore at the amorphous grain boundary; periodic bright spots are visible in the corresponding Scherzer image.

*(B) Scherzer Image Simulation of Grain Boundaries:* Some evidence for the presence of Y can be produced, however, in the traditional manner, namely, by recording lattice images at Scherzer defocus (see, for example, in Fig. 5(a)) that are then compared with image simulations. It is important to note though that Scherzer lattice images in a field emission microscope can often be misleading due to the large beam coherence and the complicated contrast transfer function. By default, less information is seen in a single lattice image than in a reconstructed image because the CTF removes information and creates delocalization. Commonly, these effects can light up edges such that the bright spots along the boundaries could be associated with imaging artifacts.

The grain boundary model that was used for the exit-wave simulations was now used to produce simulated Scherzer images. The simulations were performed covering the ion-column density range from one Y atom every 2.8 Å to one Y atom every 19.6 Å. The specimen thickness ranged from 10 to 150 Å. A selection of the simulated images are presented in Fig. 10, where the array of images corresponds to the lower and upper end of ion-column densities (2.8, 5.6, 16.8, and 19.6 Å/Y atom) covering the thickness range from 100 to 150 Å. One can clearly see that, at the low ion-column densities, no bright spots can be discerned at any specimen thickness. Instead, for the 16.8 Å/Y-atom case, periodic bright spots can be detected and start to appear between 110 and 150 Å in specimen thickness, which are most bright at ~130–140

Å. Similar bright spots can be seen for an even lower Y-ion-column density of 19.6 Å/Y atom; however, they are not as pronounced.

This information was used to extend the interface structure model further by (i) substituting the yttrium atom with silicon atoms and (ii) leaving the position at the prism planes vacant to examine the Scherzer images that it produced. The initial results of this image simulation could be seen in Fig. 6. It is apparent that the image of the Y-containing grain boundary displays an array of double bright spots along the interface at a specimen thickness of 130 Å, resembling the experimental Scherzer defocus images in Fig. 5(a). However, only the heavy element yttrium causes such bright spots to appear along the interface. The substitution of Si for Y atoms does not cause such strong bright spots and neither does a grain boundary without any atoms positioned at the prism plane.

These simulations suggest that the bright spots might represent yttrium ions at specific atomic positions along the grain boundary. However, very careful interpretation of the Scherzer images is required because the true location of the yttrium ions may not be identical to the location of the bright spots. In fact, the location of the individual atoms can be seen on the atom position overlay which reveals that in reality the bright spots are not located directly at the interface but one half  $Si_3N_4$ -hexagon ring away from it. The appearance of the spots is a result of the combination of electrons scattering off the yttrium ions and the effects of the path of information transfer through the TEM, i.e., from lens aberrations, on the electrons.

The overall relevance of these findings is of importance since minute structural changes and transitions along the thin grain-boundary films in silicon nitride ceramics can have a marked influence on their macroscopic behavior. For example, postsintering heat treatment of  $Si_3N_4$  ceramics has been used to improve their mechanical properties, specifically by fully or partially crystallizing the amorphous triple junction regions.<sup>41,42</sup> However, since triple junctions and thin grain boundaries are interconnected, their respective transformations and chemical balances can influence each other; consequently, the atomic positions of the sintering additive ions and their structural surroundings in the grain boundaries must change. The prospect is that these changes, when examined and understood, will permit insight into mechanisms that elucidate the role of the atomic structure and bonding at the local level of the nanoscale grain-boundary films. To date, one can only propose that the local bonding character and specific structural transitions along the thin two-grain interface are responsible for the marked changes in the mechanical response. Knowledge of the precise location and the chemical and structural surrounding of these additive ions can only lead to further understanding of these key nano-/microstructural features which appear to control the properties of many ceramics.

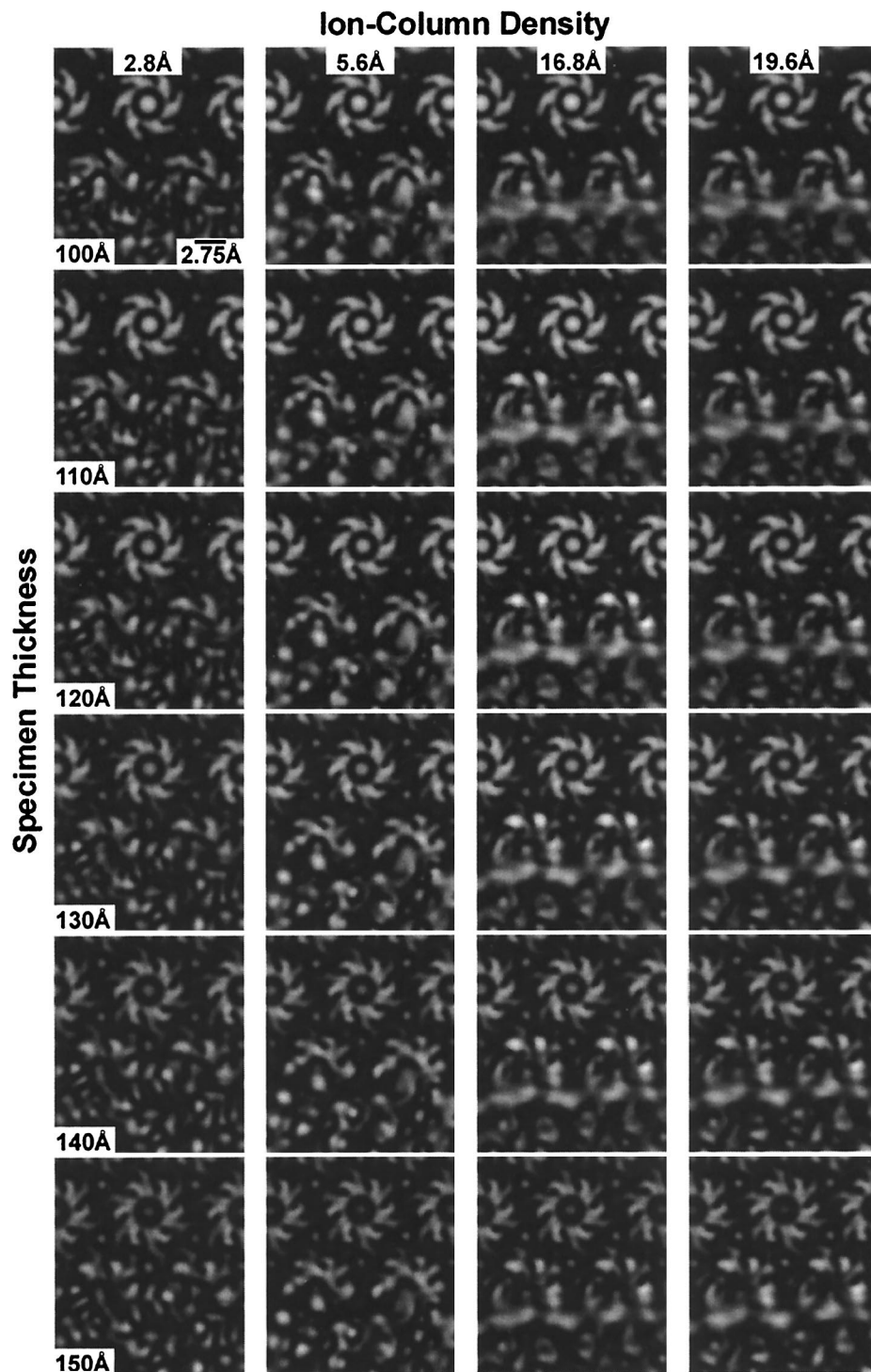


**Fig. 10.** Array of simulated Scherzer images showing the grain-boundary region containing Y at the prism planes. The emergence of periodic bright spots along the grain boundary can primarily be detected under two conditions: (i) a low yttrium ion-column density of 16.8 Å or less and (ii) a specimen thickness of  $\sim 130$  Å. The intensity of the bright spots appears to peak at this thickness.

#### IV. Conclusions

Focus-variation image-reconstruction HRTEM has been used to image the atomic structure of a silicon nitride ceramic to a resolution of 0.93 Å, i.e., close to the theoretical information limit of the microscope. Using both complementary Scherzer and exit-wave phase-reconstructed images, these techniques have been specifically applied to investigate the structure of the grain boundaries in a high-purity, dilatometer-controlled gas-pressure-sintered  $\text{Si}_3\text{N}_4$  containing 2 wt%  $\text{Y}_2\text{O}_3$  as a sintering additive.

Based on complementary EDS studies, it was confirmed that the yttrium ions had segregated to, and were present in, the grain boundaries. From theoretical studies in the literature,<sup>8–11</sup> the precise location of these ions has been assumed to be at the nitrogen (or oxygen)-terminated plane of the half-ring of the Si hexagon, i.e., on the prism-plane–grain-boundary interface; in addition, most of the yttrium atoms were expected to be located in the thin amorphous film along the boundary.

Images of a thin ( $<100$  Å) two-grain boundary resulted in a clear view of  $\text{Si}_3\text{N}_4$  half-rings reaching into the amorphous grain

boundary, suggesting that yttrium could indeed attach to those locations. However, *direct* proof via HRTEM imaging could not be obtained. Instead, image simulations helped explain why yttrium ions could not be seen at these specimen thicknesses. Specifically, the yttrium ion-column density is too low, i.e., less than one yttrium every 16.8 Å, to produce a Y signal that is below the correlated noise of the amorphous part of the interface.

Scherzer images from a thicker specimen (>100 Å) revealed periodic bright spots along the interface that were attributed to yttrium ions positioned at the prism plane. Only indirect confirmation that yttrium ions were positioned at the half-plane of the Si hexagon was possible from computer simulations of Scherzer HRTEM images recorded at larger foil thicknesses (~130 Å). However, substitution of Si for Y atoms along the prism-plane positions did not produce similar periodic bright spots.

We conclude that most of the yttrium atoms are located in the amorphous boundary phase with only a few atoms, specifically one yttrium atom every 16.8 Å, attached to the prism plane of the matrix-grain-grain-boundary interface.

### Acknowledgments

The authors thank Chris Nelson, of NCEM, for help with some of the early HRTEM work.

### References

- <sup>1</sup>D. R. Clarke, "On the Equilibrium Thickness of Intergranular Glass Phases in Ceramic Materials," *J. Am. Ceram. Soc.*, **70** [1] 15–22 (1987).
- <sup>2</sup>C. M. Wang, X. Pan, M. J. Hoffmann, R. M. Cannon, and M. Rühle, "Grain Boundary Films in Rare-Earth-Glass-Based Silicon Nitride," *J. Am. Ceram. Soc.*, **79** [3] 788–92 (1996).
- <sup>3</sup>H. Gu, X. Pan, R. M. Cannon, and M. Rühle, "Dopant Distribution in Grain-Boundary Films in Calcia-Doped Silicon Nitride Ceramics," *J. Am. Ceram. Soc.*, **81** [12] 3125–35 (1998).
- <sup>4</sup>D. R. Clarke, T. M. Shaw, A. P. Philipse, and R. G. Horn, "Possible Electrical Double-Layer Contribution to the Equilibrium Thickness of Intergranular Glass Films in Polycrystalline Ceramics," *J. Am. Ceram. Soc.*, **76** [5] 1201–204 (1993).
- <sup>5</sup>H. J. Kleebe, M. K. Cinibulk, R. M. Cannon, and M. Rühle, "Statistical Analysis of the Intergranular Film Thickness in Silicon Nitride Ceramics," *J. Am. Ceram. Soc.*, **76** [8] 1969–77 (1993).
- <sup>6</sup>H. J. Kleebe, M. K. Cinibulk, I. Tanaka, J. Bruley, R. M. Cannon, D. R. Clarke, M. J. Hoffmann, and M. Rühle, "High-Resolution Electron Microscopy Observation of Grain-Boundary Films in Silicon Nitride Ceramics," pp. 65–77 in *Materials Research Society Symposium Proceedings*, Vol. 287. Edited by I.-W. Chen, P. F. Becher, M. Mitomo, G. Petzow, and T.-S. Yen. Materials Research Society, New York, 1993.
- <sup>7</sup>C. M. Wang, X. Pan, H. Gu, G. Duscher, M. J. Hoffmann, R. M. Cannon, and M. Rühle, "Transient Growth Bands in Silicon Nitride Cooled in Rare-Earth-Based Glass," *J. Am. Ceram. Soc.*, **80** [6] 1397–404 (1997).
- <sup>8</sup>P. Dudesek and L'. Benco, "Cation-Aided Joining of Surfaces of  $\beta$ -Silicon Nitride: Structural and Electronic Aspects," *J. Am. Ceram. Soc.*, **81** [5], 1248–54 (1998).
- <sup>9</sup>L'. Benco, "Chemical Bonding at Grain Boundaries: MgO on  $\beta$ -Si<sub>3</sub>N<sub>4</sub>," *Surf. Sci.*, **327**, 274–84 (1995).
- <sup>10</sup>T. Nakayasu, T. Yamada, I. Tanaka, H. Adachi, and S. Goto, "Calculation of Grain-Boundary Bonding in Rare-Earth-Doped  $\beta$ -Si<sub>3</sub>N<sub>4</sub>," *J. Am. Ceram. Soc.*, **81** [3] 565–70 (1998).
- <sup>11</sup>G. S. Painter, P. F. Becher, and W. A. Shelton, Oak Ridge National Laboratory, Oak Ridge, TN, private communication, 2002.
- <sup>12</sup>K. Kaneko, M. Yoshiya, I. Tanaka, and S. Tsunekawa, "Chemical Bonding of Oxygen in Intergranular Amorphous Layers in High-Purity  $\beta$ -SiC Ceramics," *Acta Mater.*, **47** [4] 1282–87 (1999).
- <sup>13</sup>M. Yoshiya, I. Tanaka, and H. Adachi, "Energetical Role of Modeled Intergranular Glassy Film in Si<sub>3</sub>N<sub>4</sub>-SiO<sub>2</sub> Ceramics," *Acta Mater.*, **48**, 4641–45 (2000).
- <sup>14</sup>M. Yoshiya, K. Tatsumi, I. Tanaka, and H. Adachi, "Theoretical Study on the Chemistry of Intergranular Glassy Film in Si<sub>3</sub>N<sub>4</sub>-SiO<sub>2</sub> Ceramics," *J. Am. Ceram. Soc.*, **85** [1] 109–12 (2002).
- <sup>15</sup>H. D. Ackler and Y. M. Chiang, "Model Experiment on Thermodynamic Stability of Retained Intergranular Amorphous Films," *J. Am. Ceram. Soc.*, **80** [7] 1893–96 (1997).
- <sup>16</sup>C. Kisielowski, E. C. Nelson, C. Song, R. Kilaas, and A. Thust, "Aberration Corrected Lattice Imaging with Sub-Ångström Resolution," *Microsc. Microanal.*, **6**, 16–17 (2000).
- <sup>17</sup>A. Ziegler, C. Kisielowski, and R. O. Ritchie, "Imaging of the Crystal Structure of Silicon Nitride at 0.8 Ångström Resolution," *Acta Mater.*, **50** [3] 565–74 (2002).
- <sup>18</sup>M. A. O'Keefe, C. J. D. Hetherington, Y. C. Wang, E. C. Nelson, J. H. Turner, C. Kisielowski, J. O. Malm, R. Mueller, J. Ringnald, M. Pam, and A. Thust, "Sub-Ångström High-Resolution Transmission Electron Microscopy at 300 kV," *Ultramicroscopy*, **89** [4] 215–41 (2001).
- <sup>19</sup>C. Kisielowski, C. J. D. Hetherington, Y. C. Wang, R. Kilaas, M. A. O'Keefe, and A. Thust, "Imaging Columns of the Light Elements C, N, and O with Sub-Ångström Resolution," *Ultramicroscopy*, **89** [4] 243–63 (2001).
- <sup>20</sup>H. Lichte, "Electron Holography I. Can Electron Holography Reach 0.1 nm Resolution?," *Ultramicroscopy*, **47** [1–3] 223–30 (2001).
- <sup>21</sup>D. Van Dyck, M. Op de Beeck, and W. M. Coene, "A New Approach to Object Wavefunction Reconstruction in Electron Microscopy," *Optik (Jena)*, **93**, 103–109 (1993).
- <sup>22</sup>W. M. J. Coene, G. Janssen, M. Op de Beeck, and D. Van Dyck, "Phase Retrieval through Focus Variation for Ultra-Resolution in Field-Emission Transmission Electron Microscopy," *Phys. Rev. Lett.*, **69** [26] 3743–46 (1992).
- <sup>23</sup>M. Op de Beeck, D. Van Dyck, and W. M. J. Coene, "Wave Function Reconstruction in HRTEM; The Parabola Method," *Ultramicroscopy*, **64** [1–4] 167–83 (1996).
- <sup>24</sup>E. J. Kirkland, "Improved High-Resolution Image Processing of Bright Field Electron Micrographs I. Theory," *Ultramicroscopy*, **15** [3] 151–72 (1996).
- <sup>25</sup>E. J. Kirkland; "Nonlinear High Resolution Image Processing of Conventional Transmission Electron Micrographs"; pp 139–54 in *Scanning Microscopy, Supplement 2*, Proceedings of the 6th Pfefferkorn Conference on Image and Signal Processing in Electron Microscopy (Niagara Falls, Canada). Edited by J. Fairing. SEM Inc., AMF O'Hare, IL, 1988.
- <sup>26</sup>W. O. Saxton, "Correction of Artifacts in Linear and Nonlinear High Resolution Electron Micrographs," *J. Microsc. Spectrosc. Electron.*, **5**, 665–74 (1980).
- <sup>27</sup>M. Op de Beeck and D. Van Dyck, "Direct Structure Reconstruction in HRTEM," *Ultramicroscopy*, **64** [1–4] 153–65 (1996).
- <sup>28</sup>D. Van Dyck, H. Lichte, and K. D. van der Mast, "Sub-ångström Structure Characterization: The Brite-Euram Route Towards One Ångström," *Ultramicroscopy*, **64** [1–4] 1–15 (1996).
- <sup>29</sup>A. H. Buist, A. van den Bos, and M. A. O. Miedema, "Optimal Experimental Design for Exit Wave Reconstruction from Focal Series in TEM," *Ultramicroscopy*, **64** [1–4] 137–52 (1996).
- <sup>30</sup>D. Tang, H. W. Zandbergen, J. Jansen, M. Op de Beeck, and D. Van Dyck, "Fine-Tuning of the Focal Residue in Exit-Wave Reconstruction," *Ultramicroscopy*, **64** [1–4] 265–76 (1996).
- <sup>31</sup>A. Thust, M. H. F. Overwijk, W. M. J. Coene, and M. Lentzen, "Numerical Correction of Lens Aberrations in Phase-Retrieval HRTEM," *Ultramicroscopy*, **64** [1–4] 249–64 (1996).
- <sup>32</sup>W. M. J. Coene, A. Thust, M. Op de Beeck, and D. Van Dyck, "Maximum-Likelihood Method for Focus-Variation Image Reconstruction in High Resolution Transmission Electron Microscopy," *Ultramicroscopy*, **64** [1–4] 109–35 (1996).
- <sup>33</sup>A. Thust, W. M. J. Coene, M. Op de Beeck, and D. Van Dyck, "Focal-Series Reconstruction in HRTEM: Simulation Studies on Non-Periodic Objects," *Ultramicroscopy*, **64** [1–4] 211–30 (1996).
- <sup>34</sup>M. J. Hoffmann, A. Geyer, and R. Oberacker, "Potential of the Sinter-HIP-Technique for the Development of High-Temperature Resistant Si<sub>3</sub>N<sub>4</sub>-Ceramics," *J. Eur. Ceram. Soc.*, **19**, 2359–66 (1999).
- <sup>35</sup>Y. C. Wang, A. Fitzgerald, E. C. Nelson, C. Song, M. A. O'Keefe, and C. Kisielowski, "Correction of the Three-Fold Astigmatism and Lattice Imaging with Information Below 100 pm," *Microsc. Microanal.*, **5**, 822–23 (1999).
- <sup>36</sup>The CrystalKit and MacTempas packages are both available from Total Resolution, National Center for Electron Microscopy, Lawrence Berkeley National Laboratory, Berkeley, CA.
- <sup>37</sup>M. A. O'Keefe and R. Kilaas, "Advances in High-Resolution Image Simulation"; p. 225–44 in *Scanning Microscopy, Supplement 2*, Proceedings of the 6th Pfefferkorn Conference on Image and Signal Processing in Electron Microscopy (Niagara Falls, Canada). Edited by J. Fairing. SEM Inc., AMF O'Hare, IL, 1988.
- <sup>38</sup>H. J. Kleebe, Colorado School of Mines, Metallurgical and Materials Engineering Department, Golden, CO; private communication at the Annual Meeting of the American Ceramic Society, 2001. M. K. Cinibulk, Air Force Research Laboratory, Materials and Manufacturing Directorate, Wright-Patterson Air Force Base, OH; private communication at the Annual Meeting of the American Ceramic Society, 2001.
- <sup>39</sup>D. Van Dyck and J. H. Chen, "A Simple Theory for Dynamical Electron Diffraction in Crystals," *Solid State Commun.*, **109**, 501–505 (1999).
- <sup>40</sup>C. Kisielowski, J. Jinschek, K. Mitsuishi, U. Dahmen, M. Lentzen, J. Ringnald, and T. Fliervoet, "Exit Wave Reconstruction, Cs Correction and Z-Contrast Microscopy: Comparative Strengths and Limitations," submitted to *Int. Conf. Electron. Mater.*, 15th, 2002.
- <sup>41</sup>F. Lange, B. I. Davis, and M. G. Metcalf, "Strengthening of Polyphase Si<sub>3</sub>N<sub>4</sub> Materials through Oxidation," *J. Mater. Sci.*, **18**, 1497–505 (1983).
- <sup>42</sup>M. K. Cinibulk, G. Thomas, and S. M. Johnson, "Grain-Boundary-Phase Crystallization and Strength of Silicon Nitride Sintered with a YSiAlON Glass," *J. Am. Ceram. Soc.*, **73** 1606–12 (1990). □